Encoding of electrophysiology and other signals in MR images

LARS G. HANSON, PHD, TORBEN E. LUND, MSC, CHRISTIAN G. HANSON, BSC

Danish Research Center for Magnetic Resonance

Copenhagen University Hospital Hvidovre

Denmark

Accepted for publication in Journal of Magnetic Resonance Imaging, 2006

Running title: Electrophysiology recorded by MRI

Corresponding author:

Lars G. Hanson, PhD,

Danish Research Center for Magnetic Resonance

Copenhagen University Hospital Hvidovre, dept. 340

Kettegaard Allé 30

DK-2650 Hvidovre, Denmark

Phone: +45 36 32 28 84

Fax: +45 36 47 03 02

email: larsh@drcmr.dk

Abstract

Purpose: To develop a gradient insensitive, generic technique for recording of non-MR signals by use of surplus scanner bandwidth.

Materials and Methods: Relatively simple battery driven hardware is used to transform one or more signals into radio waves detectable by the MR scanner. Similarly to the "mag stripe" technique used for encoding of soundtracks in motion pictures, the electrical signals are in this way encoded as artifacts appearing in the MR images or spectra outside the region of interest. The encoded signals are subsequently reconstructed from the signal recorded by the scanner.

Results: Electrophysiological eye and heart muscular recording (EOG and ECG) during fast echo-planar imaging is demonstrated with an expandable, modular 8-channel prototype implementation. The gradient artifacts that would normally be dominating EOG are largely eliminated.

Conclusion: The method provides relatively inexpensive sampling with inherent micro-second synchronization and it reduces gradient artifacts in physiological recordings significantly. When oversampling is employed, the method is compatible with all MR reconstruction and post-processing techniques.

Keywords: Wireless recording of electrophysiology, MRI, mag stripe signal encoding, RF modulation

1 INTRODUCTION

Recording of electrical signals in an MRI suite is generally problematic as the sampling equipment needs to be MR compatible, meaning safe, well-functioning at high field, insensitive to radio frequency waves (RF) and electromagnetically silent at MR frequencies. Such recordings may for example represent button-press responses to stimuli presented to a patient in the scanner, and they often need to be correlated with MR imaging or spectroscopy thus adding the complexity of synchronization. Recording of electrophysiological (EP) signals during MRI poses extra difficulty as the rapidly changing magnetic fields induce electrode voltages that are often orders of magnitude stronger than the weak electrical signals originating from neural activity.

A particularly demanding example is recording of electroencephalography (EEG) during fMRI (1). This combination has great potential ranging from patient supervision, over research in basic neurological processes to improved diagnosis of epilepsy (2). However, EEG recording in an MRI environment suffers extreme degradation due to pulse and imaging artifacts that are often orders of magnitude larger than the EEG signal of interest even after minimizing the presence of current loops. The imaging artifacts are induced by the strong and rapidly changing gradients used for fast imaging. In many studies EEG-recordings were therefore performed in silent periods between image acquisition. However, most methods including functional MRI (fMRI) benefits from imaging with high temporal resolution and unnecessary pauses should normally be avoided.

An EEG sampling strategy of particular interest in the present context was introduced by Anami and coworkers (3). This technique coined "stepping stone sampling" reduces imaging artifacts by recording EP signals only in periods where gradient currents are constant. It was demonstrated that EEG can be recorded with limited distortion in short periods between gradient reversals during echo-planar imaging (EPI). The method benefits from synchronization between scanner and EEG clocks (4) which facilitates filtering of residual imaging induced noise (5). Triggered 20 kHz sampling was used by Anami to record the EEG during 400 μs silent periods where also the MR signals were measured, i.e., in the periods between changes of directions of k-space-traversal in blipped EPI. This method is highly suited for fMRI.

The setup used by Anami and coworkers is fairly complicated, and relies on microsecond synchronization between scanner and EEG equipment obtained by driving the EEG-system with the scanner clock and using high bandwidth sampling and triggered sample-hold. Also, the MR sequences generally have to be edited to provide the needed triggering. After acquisition, the problem remains of

correlating EEG and MR images stored and time-stamped differently in separate computer systems.

These issues of measurement, synchronization, bandwidth and data management, are addressed in the present paper that introduces a conceptually simple method for recording of electrical signals within the MR suite. RF carriers emitted from a frequency generator are modulated by the electrical signals that are to be measured during imaging. These non-MR signals emitted within the RF enclosure are recorded by the scanner, and can subsequently be extracted from the MR raw data. Surplus bandwidth of the MR system is thereby used to record and store both MRI and electrical signals with inherent microsecond synchronization.

The encoded signals appear as stripes in the MR images somewhat similar to the magnetic stripes used for sound track encoding in motion pictures (the "mag stripe" technique). In both cases, the stripes can be positioned outside the field of view (FOV), which in the case of MR requires use of readout oversampling. When used this way, the method does not interfere with any image reconstruction or postprocessing algorithm whether linear or not.

In addition to providing a way of recording and storing any signal originating in the scanner room, the technique offers an implementation of Anamis (3) gradient artifact reduction technique. Heart and eye musculature recording, electrocardiography (ECG) and electroocculography (EOG) during echo-planar MRI at 3 tesla is demonstrated in the present paper. EOG is normally dominated by gradient noise and recording of EOG/ECG signals during rapid EPI is therefore far from trivial and is well suited for demonstration as it can be verified that the signals are measured correctly. The measurement of EOG is also relevant in itself, e.g. for limiting confounding movement correlated signal changes in fMRI and for monitoring of eye movements in visual studies.

2 Materials and Methods

The implemented setup is schematically illustrated in Fig. 1. Electrophysiological and known calibration signals are amplified and encoded onto distinct RF carriers in the frequency range detectable by the scanner. These signals are emitted as radio waves inside the RF enclosure by use of a simple aerial. The signals are thus detected by the scanner during imaging, and are encoded in the imaging or spectroscopy data from where, it can be extracted during data processing. In order to reduce bandwidth requirements and to avoid gradient and RF induced transients in the measured EP-signals, gradient activity triggered gating is implemented with a sensor coil placed near the opening of the scanner. The details of the various components are described below.

2.1 AMPLIFIER OF ELECTROPHYSIOLOGICAL ACTIVITY DURING SCANNING

An amplifier for EP-signals with selective detection (gating) and short settling time was constructed to avoid influence from RF pulses and magnetic field changes that could saturate the circuit. During echo planar MRI, the magnetic gradients change before each sampling period. This introduces a short but very powerful unwanted signal, decades stronger than the EP-signal. The EP- and MR signals were sampled and held when transients from the magnetic gradient change had died out.

To trigger the gating circuit, a gradient activity sensor was placed at a fixed position near the opening of the scanner. It consisted of loops of wiring forming a simple, balanced hand-wound coil (60 windings, 5 cm diameter) over which a voltage was induced by gradient changes. A high filter bandwidth of 1 MHz for the gating ensured that also abrupt gradient changes were detected. After approximately 100 μs of silence following periods of activity (sufficient for the electrode signal to settle), the gating circuit was opened for around 20 μs. A 10 kHz low-pass filter is associated with the input, and the noise level therefore corresponds to 100 μs signal averaging per sample of the undistorted signals. The filter leaves signals at frequencies below 625 Hz essentially undistorted. In total, the delay from gradient activity to sampling was approximately 120 μs which is shorter than the period between gradient reversals even for fast EPI with an echo spacing of say 500 μs. The exact timing is not critical, as long as the amplifier has time to settle. Consequently sampling with practically any plateau-sampling EPI sequence is feasible with no adjustment of the sequence or constructed hardware.

After amplification by an adjustable factor ($\times$1600-14600 allowing input ranges of 300 μV to 3 mV, full scale), the signal was offset and scaled to ensure an always positive sign for the dynamic range of interest. This resolves sign ambiguity in subsequent demodulation steps.

2.2 RF ENCODING

The RF signal encoding was performed using a specially designed multi-frequency amplitude modulator, consisting of a common reference oscillator and eight oscillators providing different frequency offsets for each of eight channels.

The reference oscillator was made with a voltage controlled crystal oscillator and a low jitter programmable phase locked loop (PLL). The clock for each channel was obtained by another low jitter programmable PLL. This gives the advantage of easy adjustment to the MR frequency range and frequency drifts well below levels of significance. The drift between channels is negligible whereas

for the common frequency, a 5 ppm (parts per million) slow temperature dependent drift limited to the first 5 minutes of operation was observed. The equipment works with scanning between 1.5 and 250 MHz with roughly 10 ppm resolution (proton scanning up to 5.8 tesla). The digital output from each PLL was bandpass filtered to avoid problems from higher harmonics. The frequencies of operation were chosen within the bandwidth of the scanner and its filters, but outside the frequency range of the MR signals.

The channel clock and the filtered signals were fed to the amplitude modulators. The outputs from these were joined in a power combiner and sent to the RF output with a transmitter power of approximately 10 nW per channel. The aerial was a simple quarter wavelength flexible wire extending horizontally from the modulator box.

Any of the eight channels can be individually switched to transmit different artificially generated step-function signals rather than measured signals. These signals generated internally in the modulator box were used for calibration, validation and demonstration purposes, but could also be used to verify, e.g., EPI timing.

2.3 SAMPLING AND DECODING

Images acquired while the modulator is active in the scanner room appear normal except for patterns along lines orthogonal to the frequency encoding (readout) direction. Depending on the chosen frequencies, these lines may only be visible when the total bandwidth is increased. With appropriate adjustment, the image of the scanned subject is undistorted.

Image acquisition using echo planar imaging involves high bandwidth sampling, typically around 100 kHz for approximately 100 ms. Often, the sampling period is split into shorter periods, one per line of the image. In contrast to the MR signals, the signals emitted from the modulator are not directly influenced by changing magnetic fields. With the chosen encoding (amplitude modulation at distinct frequencies), the encoded signals can consequently be extracted from a spectrogram of the measured data. It is simple and fast to calculate a spectrogram for each image, i.e., the frequency content as a function of time. This is most easily done by organizing the measured data in a matrix similar to the k-space data matrix used for image reconstruction, but with time along both axis (”true” time, and time from last beginning of a sample period). For the case of EPI, this matrix is identical to the k-space data matrix except for a reversal of every second line, and possibly an apodization. In order to calculate the spectrogram, the matrix is Fourier transformed along the ”short” time axis, and the

phase is discarded.

The squares of the offset and encoded signals were reconstructed with time resolution equal to the EPI echo spacing by averaging of a small number of neighboring columns of the squared absolute spectrogram. From these, the offset and scaled signals were recovered. Comparison to the simultaneously acquired known calibration signals can establish the original signal including sign and magnitude.

This analysis was done on a separate PC using locally developed software implemented in the programming language IDL (Research Systems Inc., Boulder, Colorado, USA). The raw MR data and acquisition parameters were automatically saved on the MR acquisition computer and were copied via network to the separate PC. The implemented software subsequently extracts a given number of embedded signals from the EPI raw data, and performs basic analysis. The timing information was derived from the transferred acquisition parameters. The carrier frequencies were derived automatically from the raw data itself by analysis of the power profile averaged over all EPI readouts. The carriers may not have the most power, but since they give rise to sharp peaks in the spectral distribution, they were consistently found to have the most pronounced power difference compared to the neighboring frequencies (pixels). Consequently, the carriers were detected at the distinct positions with the smallest second derivatives (negative) of the averaged power profile. The frequency range used for integration was not critical, but was chosen to be ± 6 kHz (3 pixels on either side of the detected peak).

2.4 MRI PROTOCOL AND SETUP

For demonstrating the technique, a simple and illustrative setup was chosen. The gradient echo product sequence of the a 3 Tesla, whole-body imaging system (Siemens Trio, Erlangen, Germany) was used for repeated echo planar imaging of three axial slices through the eye region of a healthy volunteer for 28 seconds. The standard quadrature head coil was used. In the middle third of the period, the subject paused with open eyes, whereas the remaining time was spent alternately looking right and left self-paced. This activity would normally be visible on both MR images (6) and EOG, and the correlation between the two can therefore be used to probe the validity of the approach. Electrophysiological signals were measured during MRI with MR compatible electrodes positioned near the heart and eye musculature to record ECG and EOG simultaneously. The experiments were performed after approval was granted by the local ethics committee and after informed consent was given by the

subject.

The MRI parameters were as follows: Slice thickness 5 mm with 1 mm inter-slice gap. The echo and repetition times, TE/TR=41 ms/235 ms, were chosen minimal for the used 128x128 image matrix and 400 mm quadratic FOV (3 mm is a typical fMRI in-plane resolution). Each EPI gradient lobe involved ramping up for 130 μs, a 300 μs plateau, and 130 μs ramping down. Sampling was performed in the middle 512 μs period, thus including 212 μs ramp-sampling, being unproblematic only due to the used gradient-activity triggering. The used parameters are representative of studies where emphasis is put on fMRI performance, i.e., the gradient artifacts in EP-recordings were not minimized by sacrificing temporal or spatial resolution.

2.5 Electrophysiological signal characteristics and filtering

The EPI echo spacing was 0.56 ms which is therefore also the time resolution of the EP signals measured during single-image acquisition when reconstructed as described above. Between image acquisitions, however, there are periods of excitation, spoiling and other acquisition pauses. With the used imaging parameters, there are 5 ms periods between EPI of neighboring slices, where the EP-signal was not measured. For a time domain-analysis, this would normally not require attention, but it must be considered if, e.g., the alpha-power of an EEG is to be estimated (discussed later).

In addition to the 128 readouts used for reconstruction of each EPI image, the used sequence acquires 3 reference lines for the purpose of ghost-correction. These are not phase-encoded. They contain encoded EP-signals but were discarded from the EP-signal reconstruction to avoid potential transients in the beginning of the EPI echo-train. The non-sampled interval therefore increased from 5 to 6.6 ms corresponding to EP-signals being measured in roughly 90% of the available time.

Due to eddy-currents and other differences between sampling on positive and negative gradient lobes (sources of normal EPI-ghosting), modulation of every second EP-sample is expected, but easily removed by filtering or by sacrificing half the bandwidth. The latter approach was chosen here as the resulting Nyquist frequency, 446 Hz, is still sufficient for sampling of all EP signals. Neighboring samples were simply averaged giving a time resolution of 2×0.56 ms $= 1.12$ ms except in the above-mentioned pauses between slices.

There may be additional signal variation with the EPI line number, e.g., from transient eddy currents from phase-encoding or slice selection gradients. This non-random noise can be estimated and filtered relatively easily (4, 7) but this was not necessary for the present application. It is likely to

be necessary for EEG recordings.

To avoid possible modulation with the slice number, e.g., coming from MR signal leakage into the EP-signal region, the data were filtered in the following way: The extracted EP-signals were averaged over each image, so the time resolution was temporarily decreased from 0.56 ms to $\mathrm{TR}/3 = 78$ ms equidistant sampling. With one sample per image, it is simple to remove oscillation in synchrony with the slice excitation by use of a filter exchanging the spectral content at frequencies $\pm 1/\mathrm{TR}$ with the means of the neighboring frequencies differing by the reciprocal of the total scanning time. Subsequently, the low-frequency part of the original high-resolution time series was exchanged with the filtered version, thus removing slice selection effects occurring at single sharp frequencies in a simple and effective way. For recording of rhythmic electrophysiological signals for short periods of time, the timing or the filtering approach may need to be reconsidered (8) if modulation is observed.

The MR images were reconstructed using 2D Fourier transformation after Gaussian smoothing in the readout direction (2 pixel full width at half maximum, sometimes used in fMRI analysis). This suppresses phase discontinuities at the edges of the acquisition matrix, thus effectively preventing side lobes of the encoded signal to leak into the MRI object region.

2.6 OVERSAMPLING

The widely used faster-than-necessary recording of MR-signals known as readout oversampling is particularly important in the present context, as this is responsible for making the technique compatible with all reconstruction and post-processing techniques. It provides a means for making the reconstructed MR images completely unaffected by the encoded signals.

For normal MRI, the adequate sampling rate is calculated as the product of the gyromagnetic ratio, the maximum readout gradient and the FOV in the readout direction. Signals and noise at frequencies outside this range are filtered to avoid aliasing. The sampling rate is often increased and the filter bandwidth adjusted correspondingly, a process known as oversampling. This corresponds to sampling signals at a rate sufficient to reconstruct images with a wider FOV than prescribed, and it has the advantage that filter edge effects responsible for image distortions are moved outside the FOV. In the initial stage of normal image reconstruction, the extreme frequencies are discarded and the FOV thereby reconstructed to the prescribed width. The technique is not associated with extra noise or other drawbacks, and the technique is therefore used routinely by scanner vendors. A factor of two oversampling is default on the used scanner.

In essence, readout oversampling provides a frequency range where the extra signals can be encoded without affecting the reconstructed images. With a proper choice of encoding frequencies, the signals are only reflected in raw data, and are removed without a chance to affect e.g. navigator echoes or ghost correction. Potentially interfering edge effects of the filter can be mapped using the calibration signal and corrected for on a per scanner basis. In the present demonstration, one signal is encoded in the oversampled frequency range (the ECG), and two in the normal MRI frequency range to illustrate the difference.

3 RESULTS

The positioning of the amplifier and modulator in the MR room proved to be easy and non-critical. Several positions were used, and no special attention to the orientation or positioning of the antenna was needed, although those parameters influence the amplitude of the measured non-MR signals. As the signals are influenced equally, the sampling of the known calibration signal provides a reference that can be used to make quantitative measurements.

The simple data extraction algorithm worked reliably, even when RF carriers were weak, or when they were overlapping with MR frequencies (in which case, of course, both MR images and EP-recordings are corrupted). Consequently, for shorter acquisition periods (less than a minute) the MR images and the EP-recordings could be viewed and correlated seconds after the acquisitions were finished with the number of EP-signals being the only parameter manually specified. For longer acquisitions, the network copying was the most time-consuming step. The following graphs are output from the software.

Figure 2 shows simultaneous brain imaging and measurement of three signals transmitted wirelessly to the scanner. The latter appear as patterns on both sides of the normal MR image, that have relatively low signal to noise ratio (SNR) due to the short TR. Oversampling is employed in the readout direction but the image is calculated from the raw data before truncation of the FOV so the width is twice the height in contrast to the quadratic images reconstructed by the scanner. Geometrical distortions due to the air-filled sinuses and nasal cavities are seen near the eyes. Nyquist N/2-ghosts being faint copies of the water image, are visible above and below this. The ghosts result from the use of a rudimentary, conventional 2D Fourier image reconstruction (i.e. no ghost-correction).

Figure 3 shows the same kind of data reconstructed differently to reveal the time evolution of the embedded signals as described in detail earlier. Starting from the raw data matrix that was Fourier

transformed to give Fig. 2, every second horizontal line was here reversed to switch from a (k_x, k_y) data representation to a representation with time along both axis $(t_{\text{short}}, t_{\text{long}})$ as k_y (the "blip" direction) is proportional to time for echo planar imaging. The shown image result from a subsequent 1D Fourier transformation along the short time axis, thus providing a spectrogram with frequency along the horizontal axis. In this representation, the MR signal present in the central 50 kHz region is too faint to be seen. The embedded signals, however, appear as stripes as they are transmitted via amplitude modulated carriers at distinct frequencies. The changing amplitude is seen as intensity variations (the EOG has too little amplitude variation for this to be clearly visible). The raw data from the whole 28 second acquisition enters the graph, so the data shown in Fig. 2 acquired over a fraction of a second, appears over a tiny fraction of the time axis.

Figure 4 shows the physiological and calibration signals extracted from the spectrogram. The high field gives rise to distortions in this ECG, but apart from this, the quality is high, considering the time resolution and that the signal is virtually unfiltered and acquired during high speed MR imaging. The middle graph is the calibration signal that consists of superimposed step functions with small and large amplitude. The top graph is the EOG showing large oscillations in the two periods with eye motion and little variation in between. Again, the quality is good considering the extreme circumstances. The local variance of the EOG correlates with the amplitude of the calibration signal, showing that channel cross talk is a limiting factor in the current implementation. This is clearly visible in the EOG during the middle period and is confirmed by examining a high pass filtered version of the EOG reflecting clearly the immediate amplitude of the calibration signal (not shown).

It remains to be shown, that the measured signals are indeed EOG and EEG. Figure 5 thus provides correlation maps between the measured EP time courses and the pixel intensities. High correlation between the EOG and the image intensity is found in the eye region, and similarly, correlation is seen between the ECG and the image intensity near the medial cerebral artery and the Circle of Willis, demonstrating the validity of the approach. High correlation is also found in other regions, most notably outside the head, as the signals are encoded as artifacts there. The signals are seen to take up more bandwidth than needed and the overall noise in the MR images is therefore increased. In contrast to Fig. 4, the time courses shown are averaged over each slice-acquisition period. They therefore have higher signal-to-noise ratio and a quality that is fully sufficient for e.g. eye motion detection.

4 DISCUSSION

As high bandwidth sampling equipment is already available in all MR suites and is reused in the proposed setup, the complexity is correspondingly limited: No extra computers or cabling into the RF cabin is needed. The equipment is small in size, weight and material price (less than 2 kg and $1000). It is low-powered and battery driven, and is not connected to the scanner or other high voltage devices. Patient safety problems are therefore minimized. The image and the electrical signals are stored together and microsecond synchronization is inherent. The program extracting the encoded electrical signals can be made part of the image reconstruction software. Signals and images can then be conveniently stored together in a common picture archiving system (PACS), as the DICOM standard used by most PACS implementations support both EP- and MR-image formats (9).

In the present implementation, the gradient artifacts were largely avoided by use of gradient activity triggered sampling. The gating circuit needs to be opened at least twice over a period of the fastest oscillatory EP signal to avoid aliasing in a frequency-domain analysis. This was ensured by avoiding long pauses between slice acquisitions. This is normally the preferred situation for fMRI anyway.

A related difference to traditional techniques is the variation in sampling rate over extended periods. Whereas independent signal values can be encoded and decoded several times per millisecond in the EPI periods lasting, e.g. 100 ms, there are relatively long periods between EPI measurement (e.g., 10 ms during excitation), where the scanner does not normally sample. For low-frequency signals such as EOG and ECG this is not a major concern, as the image sampling rate (e.g. 10 per second) is adequate. It needs to be taken into account, however, if the signal changes significantly during the pause, e.g., if the frequency exceeds approximately 100 Hz. In that case, methods such as gridding, discrete Fourier transform, Lomb-Scargle periodograms (10, 11), or Bayesian approaches (12) not requiring equidistant samples must be considered for estimating the frequency content.

In the description of the EP-signal extraction, it was implicitly assumed that the original EP-signal and therefore the amplitude of the RF carrier, did not change significantly during the line sampling time (512 μs). However, the spectrogram can be calculated from other groupings of the data along the two time axis, thus allowing a trade-off of time-resolution for spectral resolution.

Channel cross-talk was found to be a limiting factor in the present implementation when the carrier frequencies were close as was the case for the EOG and calibration signal. This non-fundamental problem can be addressed by equipping each channel with a filter.

In contrast to the MR signal that is normally peaked around the center of k-space, the extra signals

are equally distributed over time and thus also over the acquisition matrix. There is consequently little or no need for extra raw data dynamic range for the encoded signals. In contrast, the encoded signals appear relatively localized in image space, and the scaling of pixel intensities should therefore preferably be adjusted to the MR signal rather than to the encoded signals. This is ensured by choosing the RF carriers for the encoded signals at oversampled frequencies.

The images presented here were processed and Fourier transformed offline whereas the corresponding images generated from the scanner were not shown. The most significant difference lies in the width of the image as the scanner employs at least a factor of two oversampling to avoid distortions at the edge of the FOV. As described in section 2.6 this implies that interference of the extra signals with e.g., scaling, ghost- and motion-correction can be avoided altogether, but with the present choice of parameters only the ECG signal appeared sufficiently far from the MR frequencies (100 kHz) to not influence the normal quadratic FOV images calculated by the scanner. This was verified in a number of experiments involving a standard signal generator (details are not given here). They confirmed that frequencies can be chosen such that normal MR images are undistorted. They also demonstrated that neither SNR, nor dynamic range, are limitations.

EPI ramp-sampling was employed, but the method nevertheless provided EP-recordings almost free of gradient artifacts. This difference to the Anami paper results from the use of triggering the sample-hold circuit by a gradient-activity sensor rather than a control signal generated by the scanner at the beginning of each sample period. The Anami setup is likely to benefit from use of a similar trigger minimizing the need for sequence adaption and timing control. Correspondingly, the gradient activity trigger is not strictly required with the presented technique, if ramp-sampling is avoided. The implementation of filters removing artifactual signal variation within each millisecond readout period is facilitated by a number of circumstances: The distortions are relatively small (3), the signals are sampled with microsecond time-resolution in perfect synchrony with gradient activity, and artifacts generated by the oscillating readout gradient are similar for the large number of k-space lines acquired over even short intervals allowing adaptive filters to become accurate rapidly (e.g. 100 ms).

Two sources of noise were removed by simple filtering: The modulation between alternating readouts acquired with opposite gradient direction, and the modulation with slice number. Both sources of noise were verified to be significant, but smaller than the signal amplitude (data are not shown). This is in sheer contrast to methods where periods with gradient activity are used for EP recording. Filtering algorithms have been developed to remove imaging artifacts, but the shot-to-shot variation

that is effectively proportional to the noise amplitude is limiting for their performance. With the presented technique, advanced filtering is therefore expected to give much improved results compared to situations where noise is dominant in the raw data. Signal distortions other than those resulting from imaging (e.g. ballistocardiac contributions (1)) were both expected and found. Their removal is outside the scope of this paper. Methods that appear applicable with limited adaption exist (7, 13, 14). Again, added robustness resulting from the much reduced imaging artifact is expected.

The number of independent signals that can be measured with the method, depends on the bandwidth of the signals and the surplus bandwidth of the scanner. 10 kHz is, for example, more than sufficient per EP-recording. The used scanner has 1 MHz bandwidth per receiver channel, but part of that is used for imaging. Using a maximum gradient strength of 40 mT/m and an object size of, say, 220 mm, a maximum of 60 independent EP signals can be measured whether or not parallel imaging is used

(1 MHz$-$42.6 MHz/T$\times$40 mT/m$\times$220 mm$=$ 60×10 kHz). This suffices for demanding applications such as multi-channel EEG. If, however, some of the receiver channels are allocated to EP-recording only, many more signals can be encoded. The used scanner has a bandwidth of 1 MHz in each of 8 channels mostly used simultaneously for parallel imaging. If, for example, six of the channels not used for standard quadrature head coil imaging were wired to the modulator 600 EP-signals could be measured with this bandwidth alone.

In conclusion, a new method for measuring electrical signals originating in the scanner room has been demonstrated. For recording of electrophysiology, the method benefits from sampling in periods free of gradient switching. Results by Anami and coworkers (3) suggest that our method is promising for improving EEG-fMRI in that case. However, the scope is not limited to sequences void of ramp-sampling. Many relevant signals are not influenced by gradients, and for those that are, filtering of artifacts are much facilitated by the inherent perfect synchronization. Even though the prototype implementation leaves room for improvement, it provides ECG and EOG recording with very limited gradient artifacts during fast echo planar imaging. The quality is sufficient for most in-scanner applications such as motion detection. The equipment needed is limited both in cost, size and complexity as surplus bandwidth and storage capacity of the scanner is being used.

REFERENCES

1. Ives JR, Warach S, Schmitt F, Edelman RR, Schomer DL. Monitoring the patient's EEG during echo planar MRI. Electroencephalogr Clin Neurophysiol 1993;87(6):417–20.

2. Salek-Haddadi A, Friston KJ, Lemieux L, Fish DR. Studying spontaneous EEG activity with fMRI. Brain Res Brain Res Rev 2003;43(1):110–33.

3. Anami K, Mori T, Tanaka F, Kawagoe Y, Okamoto J, Yarita M, Ohnishi T, Yumoto M, Matsuda H, Saitoh O. Stepping stone sampling for retrieving artifact-free electroencephalogram during functional magnetic resonance imaging. Neuroimage 2003;19(2 Pt 1):281–95.

4. Cohen MS, Goldman R, Stern J, Engel J. Simultaneous EEG and fMRI made easy. In Proc. of Human Brain Mapping Annual Meeting. 2001; 6.

5. Allen PJ, Josephs O, Turner R. A method for removing imaging artifact from continuous EEG recorded during functional MRI. Neuroimage 2000;12(2):230–9.

6. Beauchamp MS. Detection of eye movements from fMRI data. Magn Reson Med 2003; 49(2):376–80.

7. Allen PJ, Polizzi G, Krakow K, Fish DR, Lemieux L. Identification of EEG events in the MR scanner: The problem of pulse artifact and a method for its subtraction. Neuroimage 1998; 8(3):229–39.

8. Hoffmann A, Jager L, Werhahn KJ, Jaschke M, Noachtar S, Reiser M. Electroencephalography during functional echo-planar imaging: Detection of epileptic spikes using post-processing methods. Magn Reson Med 2000;44(5):791–8.

9. DICOM Standards Committee, Working Group 1. Supplement 30: Waveform interchange. 2000.

10. Press W, Teukolsky S, Vetterling W, Flannery B. Numerical Recipes in C (The Art of Scientific Computing). Cambridge University Press, 1992.

11. Moody GB. Spectral analysis of heart rate without resampling. Computers in Cardiology 1993; 20:715–718.

12. Qi Y, Minka TP, Picard RW. Bayesian spectrum estimation of unevenly sampled nonstationary data, 2002. MIT Media Lab Technical Report Vismod-TR-556.

13. Bonmassar G, Purdon PL, Jaaskelainen IP, Chiappa K, Solo V, Brown EN, Belliveau JW. Motion and ballistocardiogram artifact removal for interleaved recording of EEG and eps during MRI. Neuroimage 2002;16(4):1127–41.

14. Negishi M, Abildgaard M, Nixon T, Constable RT. Removal of time-varying gradient artifacts from EEG data acquired during continuous fMRI. Clin Neurophysiol 2004;115(9):2181–92.

Figure captions

FIG. 1. The electrophysiological signals from e.g., eye and heart musculature are amplified with gradient activity (GA) triggered sample-hold, and are used to modulate the amplitude of carrier signals at distinct frequencies in the detection range of the scanner. The signals are emitted in the scanner room by a simple aerial and are recorded by the scanner along with the normal MR signal.

FIG. 2. Simultaneous acquisition of EPI image of a transversal brain slice through the eyes and three signals (ECG, EOG and calibration) transmitted wirelessly to the scanner. Patterns appearing symmetrically outside the brain reflect the encoded electrical signals. The symmetric appearance comes from every second line in k-space being acquired with opposite time ordering, thus resulting in a reversal of the frequency axis.

FIG. 3. Spectrogram calculated from all the EPI line readouts. Arrows over the graph show the carrier frequencies of ECG, calibration and EOG signals (left to right). The horizontal line across the arrows indicate the width over which the power was integrated to reconstruct the EP-signals shown in subsequent graphs. Except for holes of several milliseconds appearing near EPI excitations, the spectrogram has millisecond time resolution. The MR signal is too weak to be seen on this scale.

FIG. 4. Time courses of electrophysiological and calibration signals extracted from the MRI raw data. The time resolution is 1.12 ms except for 6.6 ms periods between EPI of neighboring slices.

FIG. 5. Matrix of cross correlation maps between the measured time courses (ECG, EOG and calibration curves, left) and the pixel intensities for each slice (bottom). The maps appear bright where there is high absolute correlation at zero delay, i.e. in the image regions where the signals are encoded, and in regions where the MR signal is correlated to the EP-signals (e.g. the eye region where pixel intensities are correlated to the EOG). Also edges of the head appear slightly bright as the head involuntarily follows the eye motion. The correlation maps are scaled differently to highlight the physiological content.

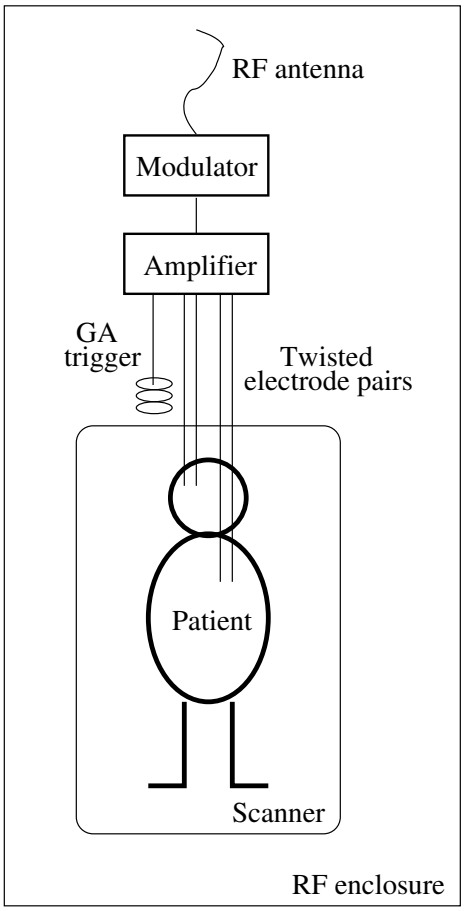

Figure 1:

The electrophysiological signals from e.g., eye and heart musculature are amplified with gradient activity (GA) triggered sample-hold, and are used to modulate the amplitude of carrier signals at distinct frequencies in the detection range of the scanner. The signals are emitted in the scanner room by a simple aerial and are recorded by the scanner along with the normal MR signal.

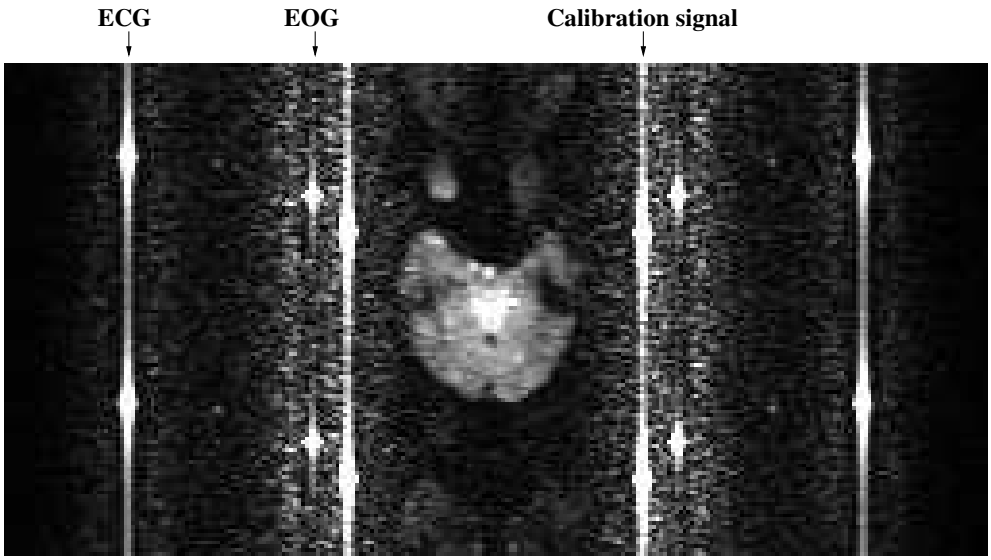

Figure 2:

Simultaneous acquisition of EPI image of a transversal brain slice through the eyes and three signals (ECG, EOG and calibration) transmitted wirelessly to the scanner. Patterns appearing symmetrically outside the brain reflect the encoded electrical signals. The symmetric appearance comes from every second line in k-space being acquired with opposite time ordering, thus resulting in a reversal of the frequency axis.

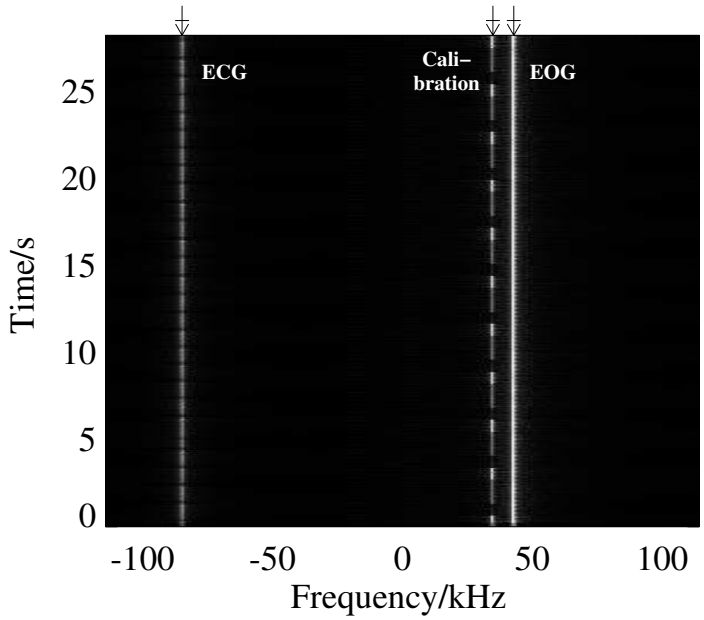

Figure 3:

Spectrogram calculated from all the EPI line readouts. Arrows over the graph show the carrier frequencies of ECG, calibration and EOG signals (left to right). The horizontal line across the arrows indicate the width over which the power was integrated to reconstruct the EP-signals shown in subsequent graphs. Except for holes of several milliseconds appearing near EPI excitations, the spectrogram has millisecond time resolution. The MR signal is too weak to be seen on this scale.

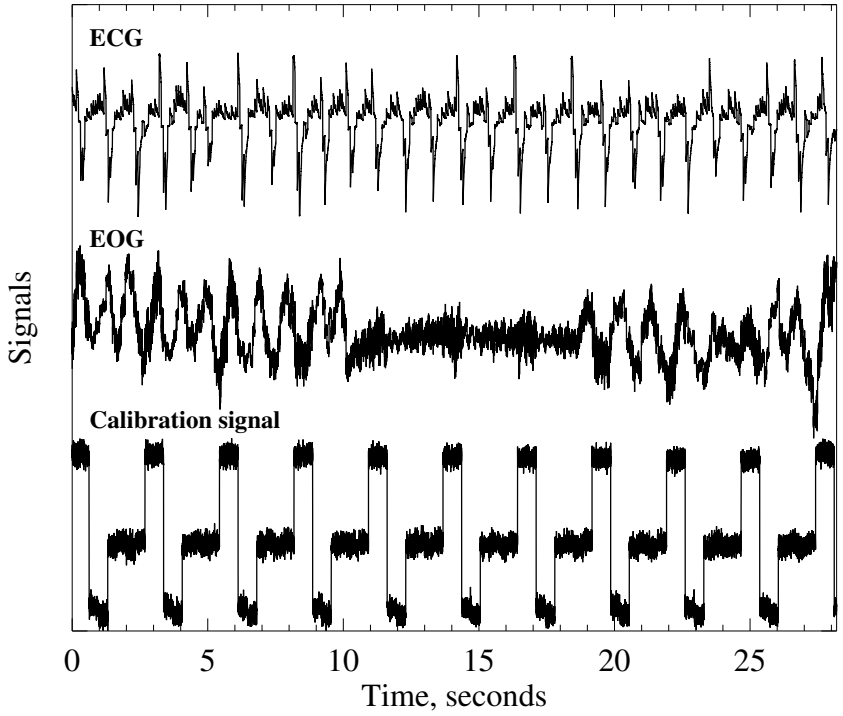

Figure 4:

Time courses of electrophysiological and calibration signals extracted from the MRI raw data. The time resolution is 1.12 ms except for 6.6 ms periods between EPI of neighboring slices.

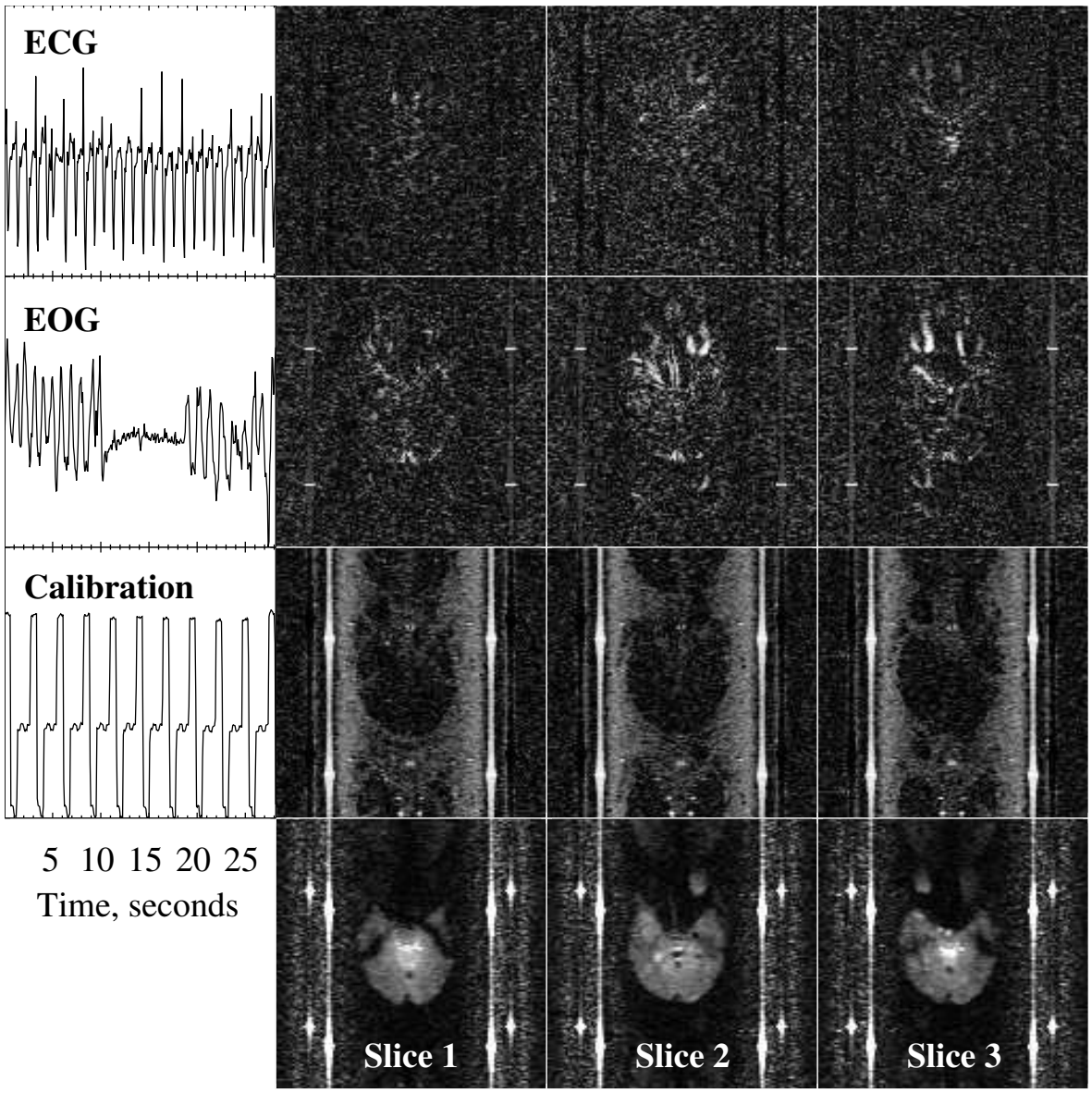

Figure 5:

Matrix of cross correlation maps between the measured time courses (ECG, EOG and calibration curves, left) and the pixel intensities for each slice (bottom). The maps appear bright where there is high absolute correlation at zero delay, i.e. in the image regions where the signals are encoded, and in regions where the MR signal is correlated to the EP-signals (e.g. the eye region where pixel intensities are correlated to the EOG). Also edges of the head appear slightly bright as the head involuntarily follows the eye motion. The correlation maps are scaled differently to highlight the physiological content.